Supporting Information

Fluorite-Structured $HfO_2/ZrO_2/HfO_2$ Superlattice Based Self-Rectifying Ferroelectric Tunnel Junction Synapse

Dong Hyun Lee,[a†] Ji Eun Kim[b†], Yong Hyeon Cho [a], Sojin Kim [c], Geun Hyeong Park [a], Hyojun Choi [a], Sun Young Lee [a], Taegyu Kwon [a], Da Hyun Kim [a], Moonseek Jeong [a], Younghwan Lee[d], Seung-Yong Lee [*c], Jung Ho Yoon [*e] and Min Hyuk Park[*a,f]

[a] Department of Materials Science and Engineering and Inter-University Semiconductor Research Center, College of Engineering, Seoul National University, Seoul 08826, Republic of Korea.

[b] Electronic Materials Research Center, Korea Institute of Science and Technology (KIST), Seoul 02792, Republic of Korea

[c] Division of Materials Science and Engineering, Hanyang University, Seoul 04763, Republic of Korea

[d] Department of Materials Science and Engineering Chonnam National University Gwangju 61186, Republic of Korea

[e] School of Advanced Materials Science and Engineering, Sungkyunkwan University, Suwon 16419, Republic of Korea

[f] Institute of Engineering Research, College of Engineering, Seoul National University, Gwanak-Ro 1, Gwanak-Gu, Seoul 08826, Republic of Korea.

†These authors have contributed equally to this work.

*Corresponding Authors: E-mail addresses: syonglee@hanyang.ac.kr, junghoyoon@skku.edu, and minhyuk.park@snu.ac.kr

Table of Contents

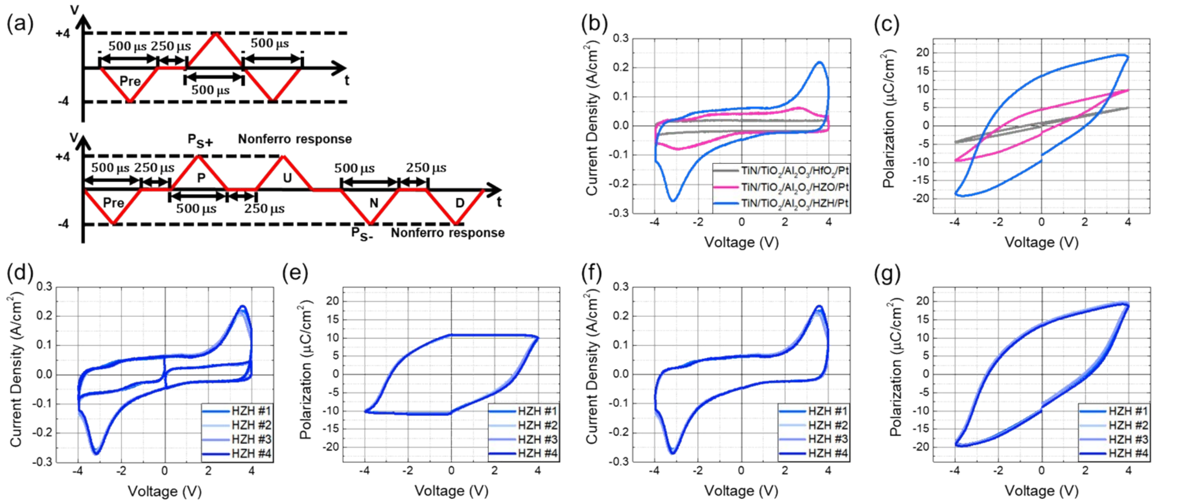

Fig. S1 (a) (Top) Bipolar triangular and (bottom) positive-up negative-down pulse (PUND) schemes used to measure polarization-voltage (P-V) curves. The measured results using triangular pulses are shown in (b) and (c) presenting current density (J) – V and P-V, respectively. (d-g) The PUND and triangular pulse measurement results at 4 different cells.

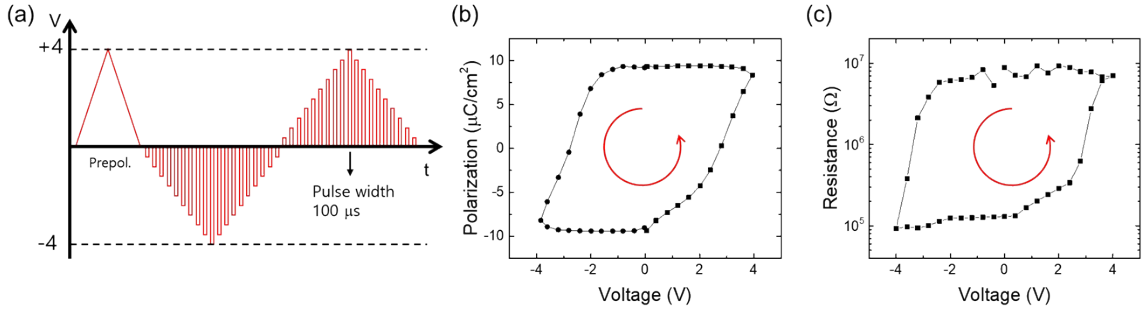

Fig. S2 (a) Pulse scheme to measure polarization and resistance modulation hysteresis. (b) Polarization – voltage curve measured after each pulse of (a). (c) Resistance - voltage curve measured after each pulse of (a). The corresponding resistance modulation depending on the polarization states shows that the device is controlled by ferroelectric polarization.

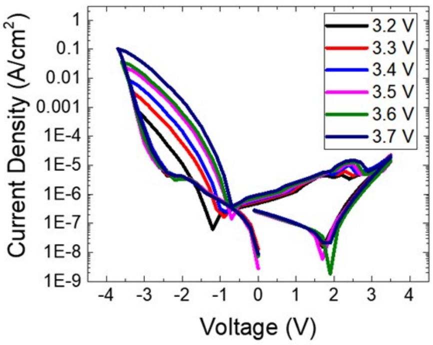

Fig. S3 Multilevel J-V curve of the device with HZH with voltage amplitude from 3.2 to 3.7 V.

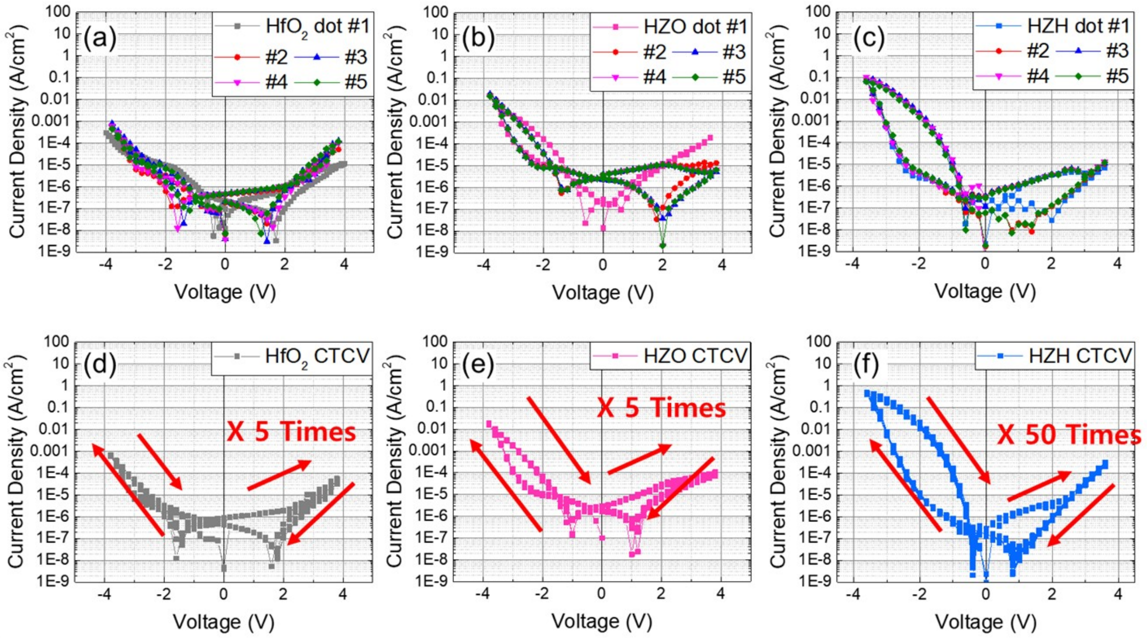

(g) σ/μ*100 (%)	HfO_2	HZO	HZH
DTDV	55.2	50.3	16.0*
CTCV	28.9	15.1	11.6

* This value is calculated using data from a 9X9 crossbar array

Fig. S4 (a-c) The measured J-V curves at 5 different points for each device with HfO_2, HZO, and HZH, respectively, show device-to-device variation (DTDV). The cycle-to-cycle variation (CTCV) was assessed with 5 cycles of DC voltage for devices with (d) HfO_2 and (e) HZO. For a precise assessment of the best-performing device, 50 cycles were conducted for the device with HZH, as shown in (f). (g) The quantitative evaluation of DTDV and CTCV by calculating the ratio of the standard deviation (σ) to the mean (μ) of the currents at -2 V.

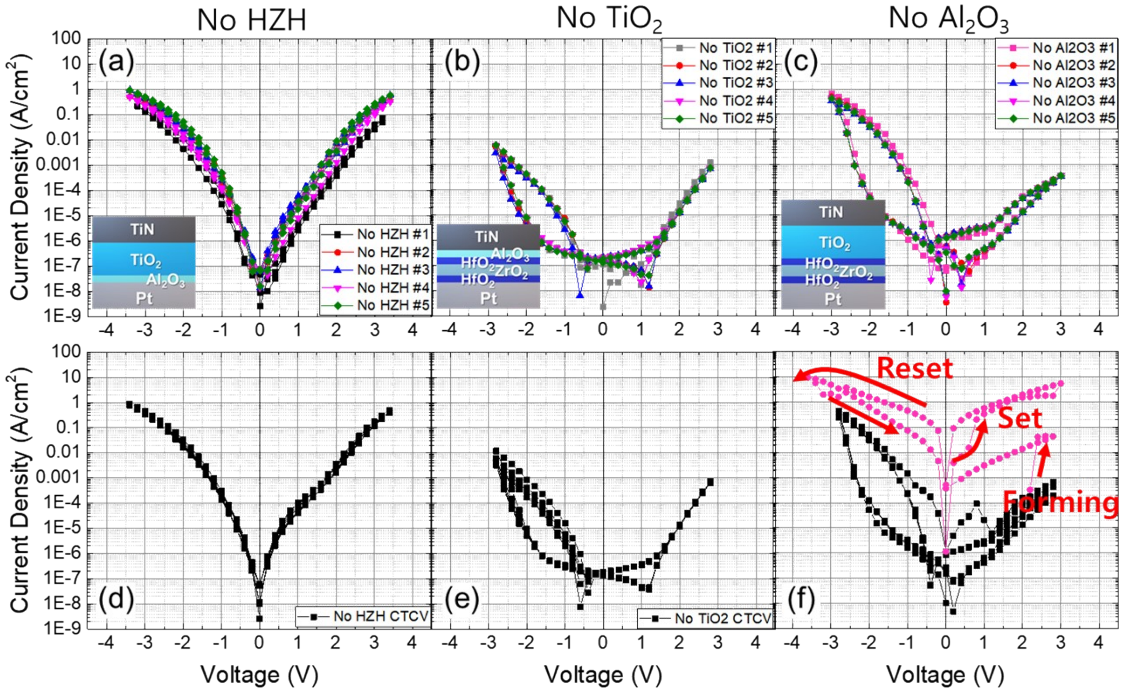

(g) σ/μ*100 (%)	No HZH	No TiO_2	No Al_2O_3
DTDV	42.1	25.7	21.3
CTCV	10.3	30.5	-

Fig. S5 (a-c) The measured J-V curves at 5 different points for each device without HZH, TiO_2, and Al_2O_3 layers, respectively. The cycle-to-cycle variation (CTCV) was assessed with 5 cycles of DC voltage for devices without (d) HZH and (e) TiO_2. In the case of the device of TiN/TiO_2(17nm)/HZH/Pt, before the end of the 5 cycles, the resistance switching mechanism was changed from ferroelectric-based to defect-based. (g) The quantitative evaluation of DTDV and CTCV by calculating σ/μ of the currents at -2 V.

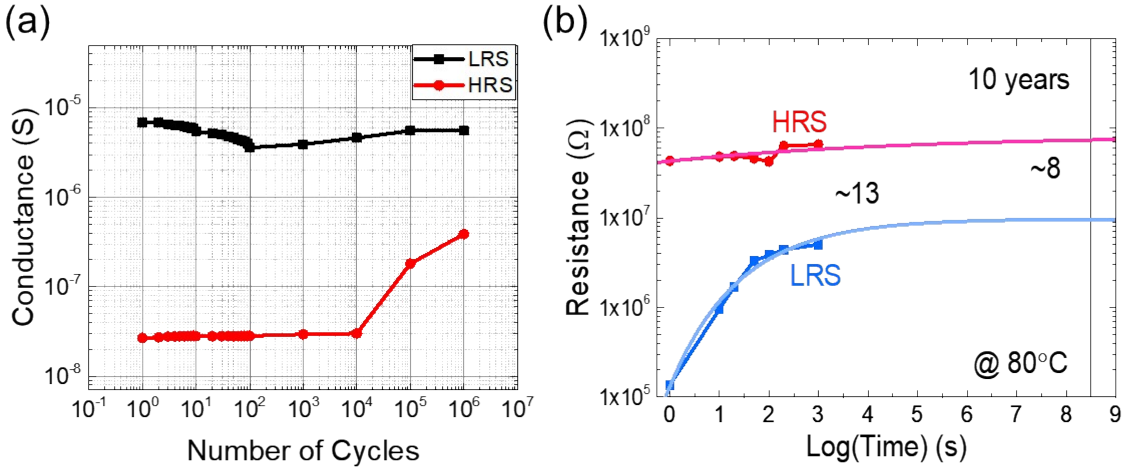

Fig. S6 (a) Endurance test conducted under ±4 V, 10 kHz square pulse stress. (b) retention test conducted at 80 °C. The retention loss in the case of the FTJs is caused by the depolarization field, which is proportional to the P_r. The retention loss in FTJs is caused by the depolarization field, which is proportional to P_r. As P_r depolarizes, the depolarization field decreases, causing significant initial loss but eventual stabilization. Domain wall speed is exponentially proportional to the field, following Merz's law. Exponential decay fitting was used for extrapolation, demonstrating that the on/off ratio can be ~8 after 10 years.

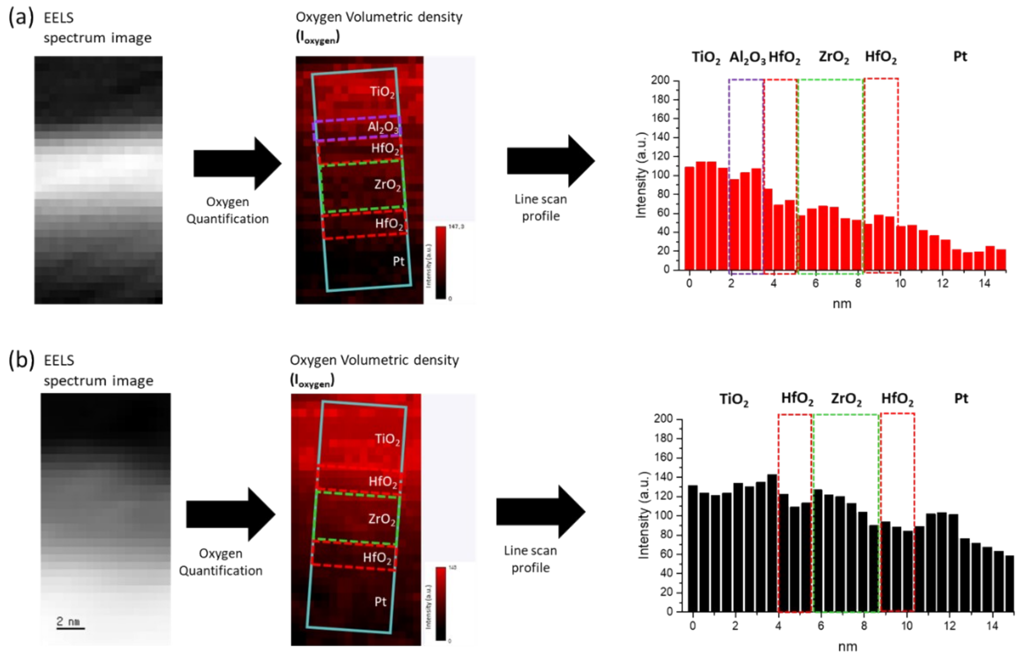

Fig. S7 Oxygen quantification using STEM-EELS. (a, b) The EELS spectrum image, the quantified map showing the volumetric density of oxygen, and the line-scan profile of quantified oxygen intensities, obtained from the sample (a) with and (b) without Al_2O_3 layer. STEM-EELS quantification was conducted using Gatan Microscopy Suite software (GMS 3), based on the method inspired by the work of Verbeeck and Van Aert.[1] Oxygen K-edge signals from 532 eV to 674 eV were used and the plural scattering effect was corrected for the quantification.

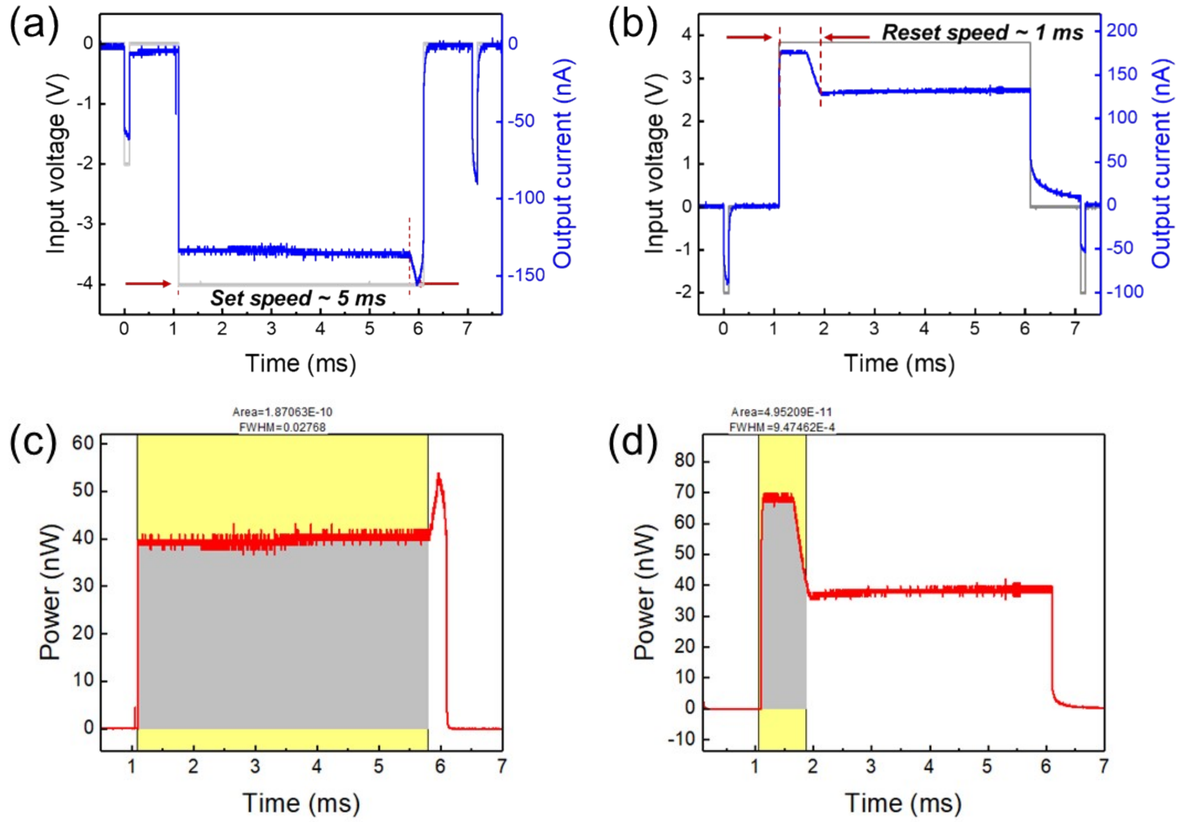

Fig. S8 (a, b) Set and Reset switching speed measurement pulse scheme and results. (c, d) Power consumption of the set and reset process measured in (a, b).

Device structure	Operation voltage	On-current	Switching speed	Rectifying ratio	Non-linearity	Ref
Ti/TiO_2/HfO_2/Si	-6 ~10 V	~100 μA	-	~ 100	~ 100	2
Pt/TaO_y/ TaO_x NP/Ta	-8 ~ 8 V	~1 μA	-	~100	~100	3
Pt/Ta_2O_5/Nb_2O_{5-x}/Al_2O_{3-y}/Ti	-10 ~ 10 V	~1 μA	10 ms	~ 1000	~100	4
ITO/NiO_X/WO_X/Pt	-6 ~ 8.5 V	~1 mA	10 ms	~ 86.9	~10	5
Au/Ti/TiO_{2-x}/Au/SiO_2/Si	-5 ~ 5 V	~10 mA	10 ms	~ 400	~ 100	6
TiN/TiO_2/Al_2O_3/HZH(6nm)/Pt	-3.8 ~ 4 V	~1 μA	5 ms	1549	94	This work

Table S1 Comparison of switching characteristics with reported self-rectifying devices.

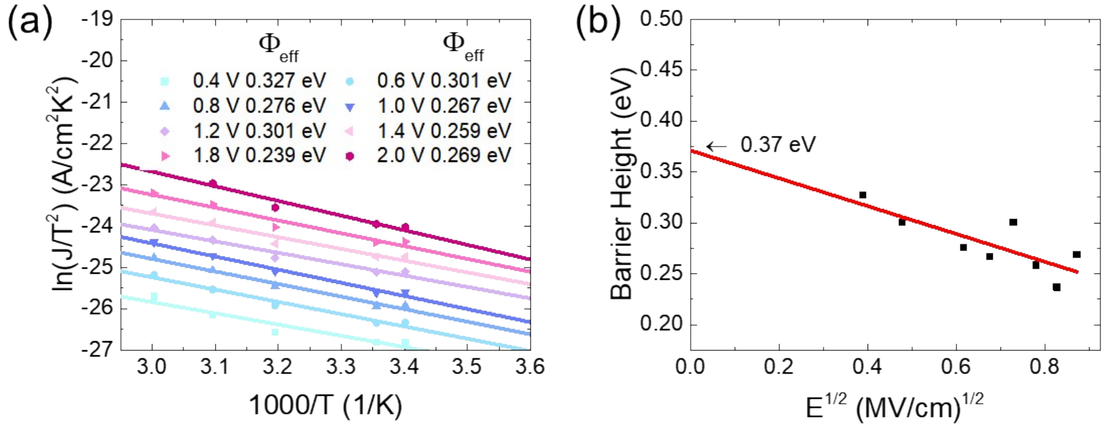

Fig. S9 (a) the ln(J/T^2) vs. 1000/T plot measured in the temperature range of 294-333K, where the slope means effective workfunction (Φ_{eff}) shown in the inset. (b) the plot of the Φ_{eff} vs. $E^{1/2}$, where the intercept means barrier height of the TiN/TiO_2 interface.

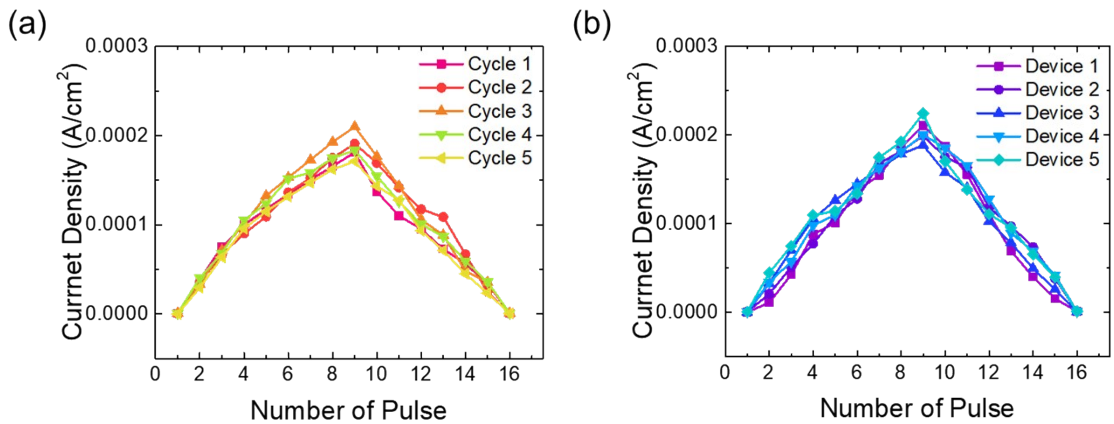

Fig. S10 (a) The resistance modulation depending on the applied number of optimized pulses in Fig. 6(b). The measurement was conducted 5 times in a single cell. (b) The resistance modulation in 5 different devices with the optimized pulses.

1 string

$(M\text{-}1)R_{s1}+R_{s2}+(N\text{-}1)R_{s3}$

Total # of R string

$(M\text{-}1)(N\text{-}1)$

Total parallel R

$$\frac{R_{S1}}{N-1}+\frac{R_{S2}}{(N-1)(M-1)}+\frac{R_{S3}}{M-1}$$

Fig. S11 Summary of equations to calculate total resistance (R) of CBA in Fig. 7(a) half-selected cells connected to the word line and bit line are R_{s1} and R_{s3}, respectively, while R_{s2} represents the other unselected cells. For the current passing through sneak current paths, the current through one of the R_{s1} is divided into (M-1)R_{s3} in parallel. This means the resistor can be considered as M-1 times larger than R_{s1}. Similarly, the currents through the R_{s3} originated from the N-1 number of R_{s1}, which means the R_{s3} can be considered as an N-1 times large R_{s3}, in terms of the current passing through any given R_{s2}. Consequently, the entire sneak current path can be presented in the (M-1)(N-1) number of strings, where one string is (M-1)R_{s1}+R_{s2}+(N-1)R_{s3}.

(a)

This Device	Ohm (GΩ)
R@V_r_HRS	710.085
R@V_r_LRS	0.558
R@V_r/2	52.213
R@V_r/3	914.627
R@-V_r/3	701.145

Assumption	Ohm (GΩ)
R_{pull}	0.6
R@linearV_r/2	0.279
R@linearV_r/3	0.186

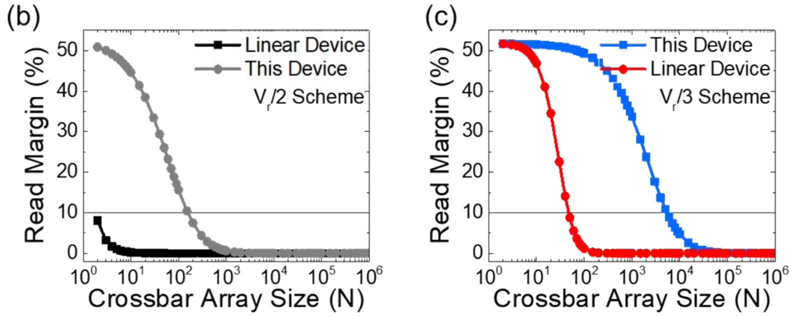

Fig. S12 (a) Upper panel shows measured resistance at each state and voltage. Except for the R@V_r_HRS, the resistances are measured in LRS. The bottom panel shows the assumed value of pull-up resistance (R_{pull}) and linear device resistance. The R@linearV_r/2 and R@linearV_r/3 are calculated resistance by dividing R@V_r_LRS with 2 and 3, respectively. (b, c) The comparison of the N × N array scalability of the device in this study and assumed linear device with parameters in (a) in which (b) shows the case with the Vr/2 scheme and (c) for the Vr/3 scheme.

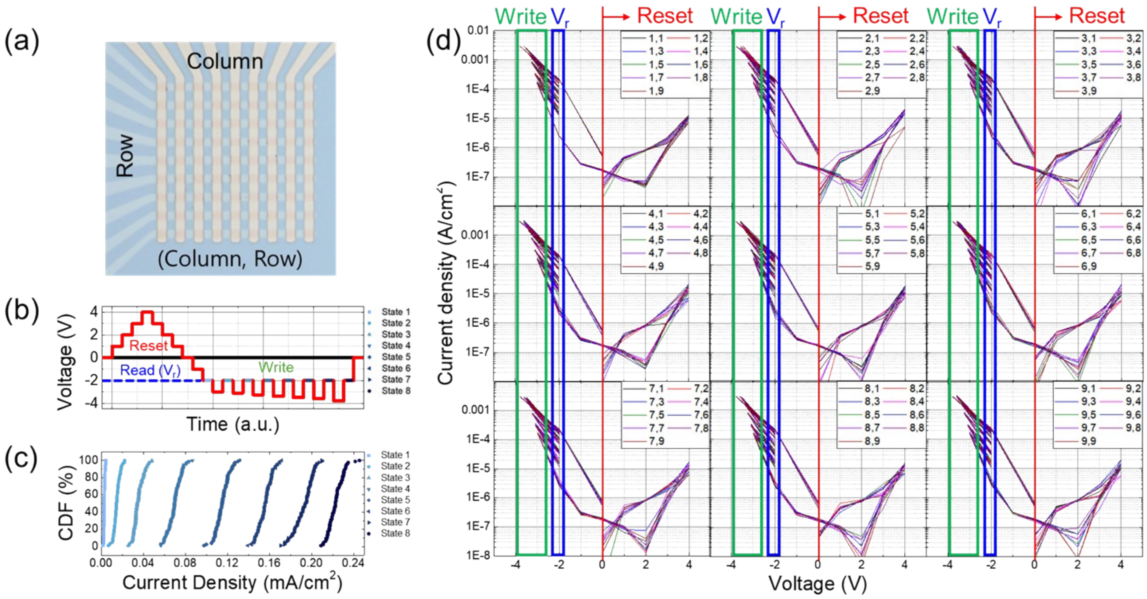

Fig. S13 (a) The coordination of the CBA. (b) Measurement scheme of 3 bits CBA cells using DC voltage application, where the applied voltage is the red line and the step for reading each state are marked with colours following the legends. In the scheme, the reset state is written in red letter, read voltage (V_r) in blue, and written in green colour. The write voltage was negative voltage with the amplitude of 3-3.8 V (c) The cumulative distribution function (CBA) of the current density taken at the -2 V in 9 × 9 CBA. (d) The entire original data of the 9 × 9 CBA data shown in Fig. 8(c). The results are separately shown column by column following the coordination numbering as shown in (a). Each reset, V_r, and write voltages are marked in red, blue, and green letters.

References

1. J. Verbeeck and S. Van Aert, *Ultramicroscopy*, 2004, **101**, 207-224.
2. Ryu, Ji-Ho, and Sungjun Kim, Chaos, Solitons & Fractals 140 (2020): 110236.
3. Choi, Sanghyeon, et al., NPG Asia Materials 10.12 (2018): 1097-1106.
4. Ren, Sheng-Guang, et al., Advanced Materials 36.4 (2024): 2307218.
5. So, Hyojin, Sungjun Kim, and Sungjoon Kim, Journal of Alloys and Compounds (2024): 175644.
6. Bousoulas, P., I. Michelakaki, and D. Tsoukalas., Thin Solid Films 571 (2014): 23-31.